Dyes and Pigments 223 (2024) 111968

Contents lists available at ScienceDirect

Dyes and Pigments

journal homepage: www.elsevier.com/locate/dyepig

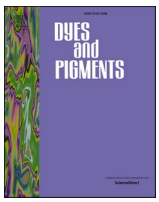

Controlling aggregation of diketopyrrolopyrroles in water

Valentina Gauci [a], Alex S. Loch [a], Daniel McDowall [a], Charlotte Edwards-Gayle [b], Dave J. Adams [a,*]

[a] School of Chemistry, University of Glasgow, Glasgow, G12 8QQ, UK
[b] Diamond Light Source, Didcot, OX11 0QX, UK

ARTICLE INFO

Keywords:
Diketopyrrolopyrrole
Aggregation
Photoresponsive

ABSTRACT

Charge repulsion can be used to control and fine tune the supramolecular aggregation of amino acid substituted diketopyrrolopyrroles in water. This is a simple method to access a number of different aggregation states with distinct photophysical properties without the need for extensive synthetic tuning, process engineering, or solvent optimisation. Most importantly, these different aggregates show different optical gaps, HOMO-LUMO gaps, electroactivity, and exciton binding energies. These systems expand the absorbance range achieved from one chromophore unit and also create systems with large Stokes shifts. This work therefore answers the demand for tailoring aggregate structures by manipulating charge repulsion in an aqueous environment.

1. Introduction

Diketopyrrolopyrroles (DPPs) are pigments that have been used in many applications including as colouring agents, in bioimaging, and in optoelectronic devices [1–6]. DPPs have become widely popular for photoresponsive applications due to their high molar extinction coefficients, high fluorescence quantum yields, large Stokes shifts, thermal and photo-stability, as well as excellent charge separation and charge carrier transport [7–11]. DPP-based systems make use of a push-pull donor-acceptor-donor (D-A-D) π-system that can be modified depending on the electron-donating groups attached (for example, thiophene or phenyl groups) [7,12,13]. Such changes allow HOMO-LUMO gap tunability which consequently effect the efficiency of exciton formation via charge separation [9,14–16]. As a result, differences in photophysical properties can be easily achieved from chemical modification [17–19]. Furthermore, the packing of such molecules into organized assemblies can contribute to further changes in the photophysical properties. This has been exemplified with nanoparticles, crystals, films, gels, and polymers [2,3,20–22]. Advantages of delocalised DPP assemblies typically include chemical stability, material robustness, and enhancement of DPP photophysical properties [6,7,23].

With regards to supramolecular assemblies, the aromatic DPP unit lends itself as a useful tool for creating assemblies via π-π stacking. The advantage of highly directional π-stacked assemblies, such as those constructed from DPPs, is the creation of a channel of intermolecular electron delocalization, referred to as the charge transfer pathway, through the π-stacked units. This delocalization runs through the entire assembled structure and thus influences charge carrier mobility throughout a material [7,21,24–30]. The efficiency of charge carrier mobility is influenced by a variety of factors, with the packing motifs of the assemblies being the most significant. For example, a more rigid and planar aromatic unit is favoured due to tighter packing and thus DPPs with appended thiophene groups are preferred over other examples [7,21]. Therefore, the mode of packing is a crucial step in designing materials for charge transfer processes as differences in aggregate orientation or packing motifs result in distinct material properties.

Different assembled structures from the same monomer can be achieved by manipulating the thermodynamic principles of the self-assembly process as exemplified by numerous cases in literature [31–33]. Overall, DPP aggregate packing is typically modified by changing phase (for example, from solution to thin film), by changing chemical structure (for example, by changing the appended aromatic group(s) on the DPP core), or by altering experimental conditions (such as solvent and temperature, or thermal annealing versus spin-coating of films) [16,29,34–44]. Furthermore, most systems are formulated using organic solvents and, despite real opportunities, there is much less investigation on aqueous-based materials. By taking advatange of the hydrophobic effect, monomers with aromatic segments can be tailored into organised structures within an aqueous medium. This additionally provides a greener approach to the formation of self-assembled systems.

* Corresponding author.
E-mail address: dave.adams@glasgow.ac.uk (D.J. Adams).

https://doi.org/10.1016/j.dyepig.2024.111968
Received 17 November 2023; Received in revised form 15 January 2024; Accepted 16 January 2024
Available online 20 January 2024

Dithiophene-functionalised DPP-based monomers (DTDPP, Fig. 1a) have previously been used to assemble fibral aggregates that create a three-dimensional network within hydrogel materials [45,46]. As is seen with similar hydrogelators, the gelation process is directed with a pH switch method (from high to low pH) where the degree of assembly and the extent of gelation vary depending on the changing pH of the system, with a significant transition point being at the apparent pK_a value (Fig. 1b) [47–49]. The degree of protonation of the carboxylic acid groups directs the packing via charge repulsion, where at a low pH (no charge repulsion) lateral aggregation of smaller fibral aggregates into tape aggregates occurs [50].

This current work takes inspiration from the previous gelation work [45], describing the formation of fluid-like colloidal dispersions instead of solid-like hydrogels. This allows the fabrication of a material with a high degree of assembly while also having the advantage of increased diffusion within the aqueous matrix that can be beneficial in certain applications [51]. The packing within the self-assembled aggregates can be controlled by changing the pH of the system while the chemical structure, phase, and external experimental conditions remain the same. Despite all systems being based on the DTDPP unit, different self-assembled structures with distinctive photophysical and electrochemical properties are formed. This results in a wide variety of supramolecular architectures and self-assembled materials that can be accessed from one monomeric template. Most importantly, this work presents significant structural changes that can be accessed by simple changes in solution conditions as opposed to the expensive and time-consuming processes explored in literature thus far.

2. Results and discussion

Four different DTDPP-R-OH monomers were examined with different amino acids substituted on the core to investigate changes stemming from the variable R group. As shown in the previously published hydrogel paper, these monomers are molecularly dissolved in organic solvents and aggregated in high pH aqueous environments (at pH 10.5) [45]. In this current work, different concentrations were used depending on the DTDPP-R-OH based on the minimum gelation concentrations (mgc) as described in the previous hydrogel work [45]. However, it is important to note that no gelation is occurring with the sol materials despite using the same concentration as the hydrogels. For DTDPP-V-OH a concentration of 10 mg/mL was used, for DTDPP-F-OH and DTDPP-A-OH, a concentration of 5 mg/mL was used, and for DTDPP-L-OH a concentration of 15 mg/mL was used. Similar to the hydrogel work, a starting sol phase at pH 10.5 was initially prepared. Pre-determined amounts of HCl were then added whilst the solution was stirred vigorously to result in the colloidal sols ranging from pH 10 to pH 2 (Table S1 in ESI). The apparent pK_a values (determined by apparent pK_a titrations) [45] of the DTDPP-R-OH derivatives vary; pH 5.5 for DTDPP-V-OH, pH 7 for DTDPP-F-OH, pH 6 for DTDPP-L-OH, and pH 5.5 for DTDPP-A-OH. The first three derivatives also have a secondary pK_a value at pH 4. A second apparent pK_a is likely due to a structural transition as has been observed for related systems [52].

Structural analysis on the aggregates dispersed throughout the sol was then carried out. Small-angle X-ray scattering (SAXS) was used to investigate the dimensions and shape of the aggregates present. Shear viscosity measurements were used to understand how the aggregate size and shape affects the mechanical properties of the different sols. Finally, absorbance spectroscopy was used to probe information on the extent of

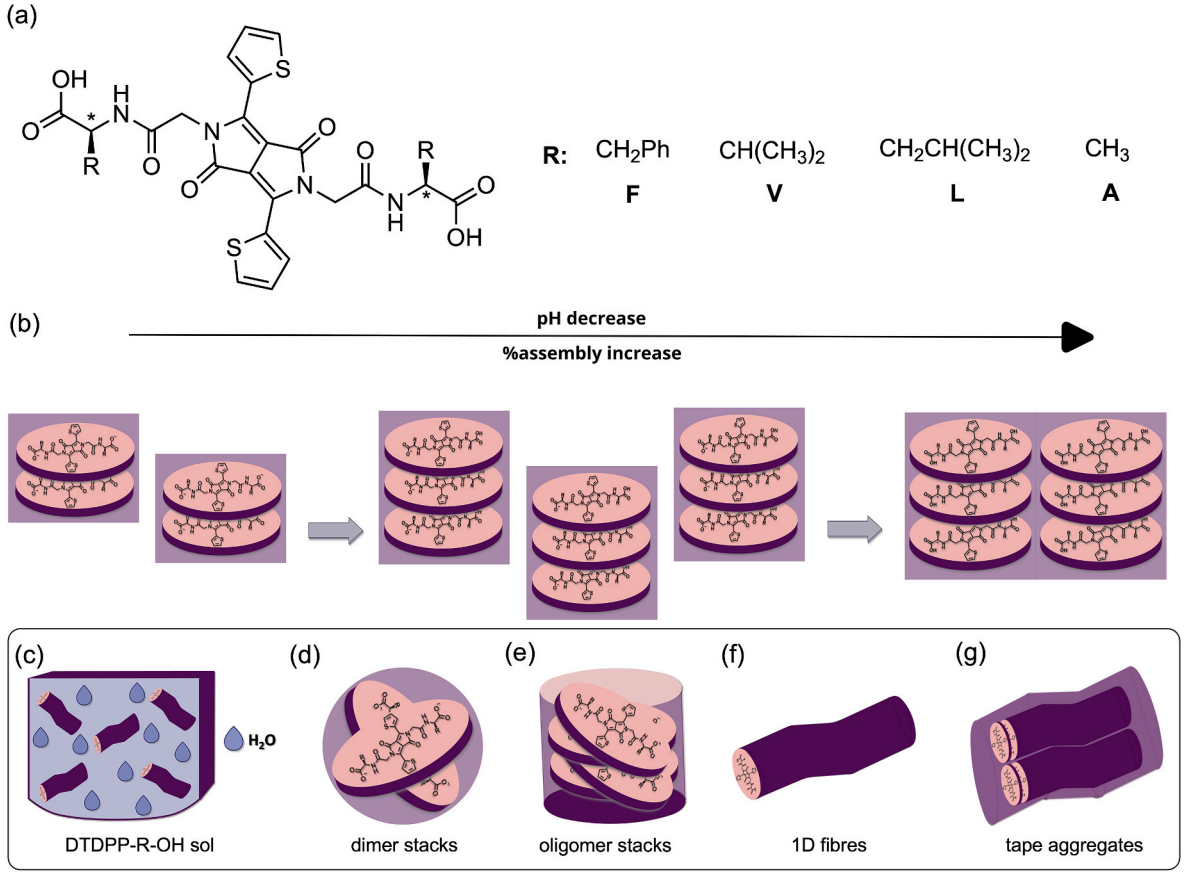

Fig. 1. (a) Chemical structure of the DPPs investigated. (b) Cartoon representation of self-assembly via a pH trigger. (c) to (g) show cartoon representations of the supramolecular architectures available from the DTDPP-R-OH monomers used here from (c) dispersed aggregates in sol material, (d) dimer stacks, (e) oligomeric stacks, (f) 1-dimensional fibres, and (g) tape-like aggregates.

aggregation within the different sol materials. As shown by the work of Kasha and Spano, the molecular orientation within the aggregates can also be probed by absorbance spectroscopy as the aggregation of chromophores can influence electronic distribution in the excited states [24, 53–57]. In essence, their work shows that electron excitation in absorbance spectroscopy leads to geometry relaxation and nuclear reorganization and thus this can distinguish between different types of stacking conformations in comparison to the monomer. Typically, H-aggregates result in hypsochromic shifts whereas J-aggregates result in bathochromic shifts. Furthermore, this can also be identified by the difference in oscillator strengths where H-aggregates have a characteristic 0-0 $<$ 0–1 vibronic peak ratio and, in contrast, J-aggregates have a 0-0 $>$ 0–1 ratio.

Focusing initially on DTDPP-V-OH, the SAXS data (Fig. 2a) show two types of behavior between the samples between pH 10 to pH 7 and pH 6 to pH 2. The higher scattering intensity for the low pH set shows that these samples contain a greater number of scatterers (Fig. S1, Supporting Information). This means that despite the DTDPP-V-OH monomer concentration remaining the same throughout the pH range, the concentration of aggregates (i.e. the degree of assembly) increases with a pH decrease. At high pH (between pH 10 and pH 7), the data is best fit to a model of a sphere in combination with a power law (Table S2 in ESI). The radius of the sphere is 15 Å to 17 Å, which is roughly equivalent to the molecular radius (Table S1, Supporting Information). This suggests that the aggregate packing at and above pH 7 is a dimer stack with the carboxylate anion groups pointing in different directions to minimise charge repulsion (Fig. 1d). For the samples from pH 6 to pH 2, the data fit best to a flexible elliptical cylinder model combined with a power law (Table S3, Supporting Information). This suggests that long fibrillar structures are formed once the system has reached the apparent pK_a and increased π-π stacking can occur (Fig. 1f). Additionally, as the fibral surface charges are diminshed at low pH, lateral aggregation of the fibral structures occurs to form tape-like aggregates (Fig. 1g). The fit parameters indicate a radius decrease on lowering the pH which is interpreted as tighter fibral packing as charge repulsion is eliminated.

The viscosity data for DTDPP-V-OH pH range also show distinctions between the high pH and low pH set (Fig. 2b and Fig. S2, Supporting Information). These data show an increase in viscosity and in shear-thinning behavior as the pH of the DTDPP-V-OH sols decreases, indicating the presence of small aggregates above pH 6 and of larger persistent entangled aggregates below pH 5. Additionally, these measurements suggest that the lower pH samples include a greater number of aggregates as was also recorded in the SAXS data. Absorbance spectroscopy shows changes in aggregation by shifts in absorbance wavelength and vibronic peak ratios (Fig. 2c and Fig. S3, Supporting Information). The spectra for the samples between pH 10 are pH 6 are identical, with an absorbance maximum at 504 nm. The sample at pH 5 exhibits a bathochromic shift of 23 nm, with the λ_{max} at 527 nm. The data for pH 4 to pH 2 are not shifted further, however, the vibronic peak ratios switch and the new λ_{max} is at 572 nm. The lower pH samples also exhibit band broadness and a 492 nm shoulder band, both indicating an increase in the degree of aggregation (as also seen in the SAXS and viscosity data). The peak ratios (Table S4 in ESI) are smaller than unity for pH 10 to pH 5 samples, and greater than unity for pH 4 to pH 2 samples. The previously published photophysical spectra of DTDPP-R-OH in organic solvents show absorbance maxima at 534 nm and 539 nm in EtOH and THF respectively [45]. In comparison to the molecularly dissolved DTDPP-V-OH, the pH 10 to pH 6 samples exhibit around a 30 nm hypsochromic shift while the pH 5 sample has around a 10 nm hypsochromic shift. The pH 4 to pH 2 samples exhibit around a 40 nm bathochromic shift.

Overall, these results indicate that there are broadly two regimes of behavior. At high pH, when charge repulsion dominates the packing, the DTDPP-V-OH is dispersed as small aggregates (i.e. dimer stacks) throughout the aqueous matrix. As the pH of the system decreases below the apparent pK_a value (at pH 5.5), removal of charge leads to increased aggregation and the formation of long fibrillar structures. Interestingly, this transition is observed first in the SAXS data at around pH 6. For the viscosity and absorbance data, a transition in behavior is seen at pH 5. This implies that the viscosity and absorbance data require a significant concentration of the fibrillar structures to be present for an effect to be observed. The formation of the fibrillar structures also necessitates a change in packing within the aggregates, with H-type aggregates present above pH 5 and J-type aggregates present below this pH.

For DTDPP-A-OH series, a similar transition occurs from small to large aggregates as the pH decreases. Fitting the SAXS data above pH 6 (Fig. 3a, Fig. S4 and Table S5, Supporting Information) suggests the formation of either dimer stacks or oligomer stacks (Fig. 1d and e). This extended stacking at high pH could be due to the smaller R group that allows tighter packing. At low pH, the SAXS data suggests fibral structures and a greater concentration of aggregates dispersed through the sol (Table S6, Supporting Information). The viscosity data show a transition from low to higher viscosity values at around pH 5, indicating a greater number of structures below the apparent pK_a value as suggested by the SAXS data (Fig. 3b and Fig. S5, Supporting Information). Interestingly, for DTDPP-A-OH, absorbance spectroscopy (Fig. 3c and Fig. S6, Supporting Information) does not suggest a transition from H- to J-type aggregates as the vibronic peak ratio is smaller than unity throughout the entire pH range (Fig. S7 and Table S7, Supporting Information). This shows that it is not always the case that the formation of specific types of aggregates leads to H- or J-aggregation. For DTDPP-L-OH range, H-type dimer stacks are present above pH 6 and J-type aggregates from pH 5 to pH 2 (Fig. 3c, Figs. S8–S9 and Table S8, Supporting Information). The viscosity (Fig. 3c and Fig. S10, Supporting Information) and SAXS (Fig. 3a, Fig. S11 and Tables S9–S10, Supporting Information) data also show a change in aggregation above and below the apparent pK_a with

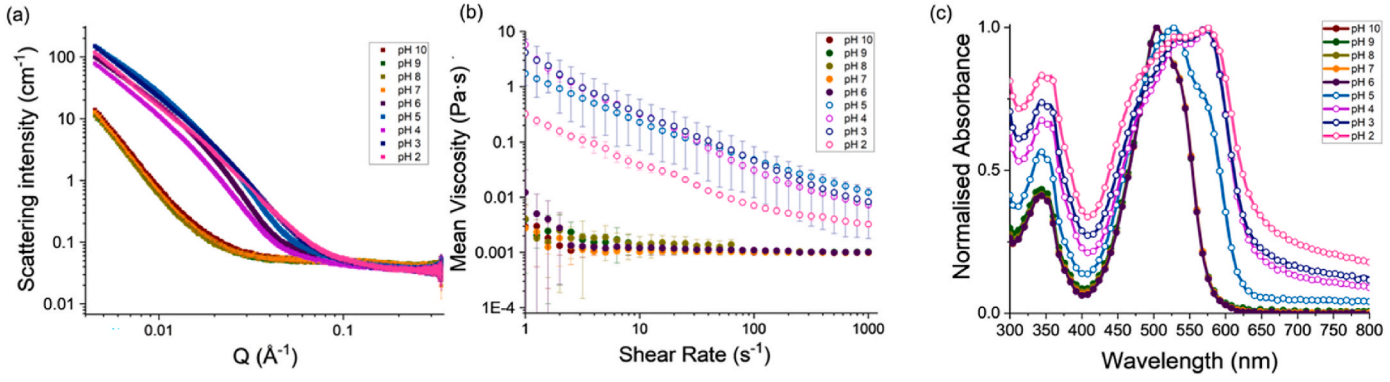

Fig. 2. DTDPP-V-OH pH range (a) SAXS data; (b) viscosity measurements (error bars based on triplicate runs); (c) normalized absorbance spectra (recorded using a 0.01 mm path length cuvette).

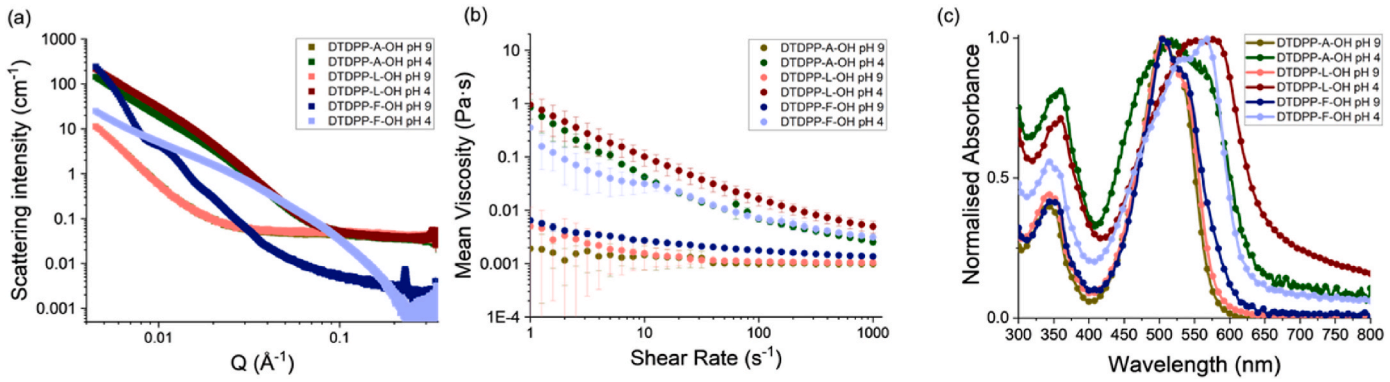

Fig. 3. (a) SAXS data; (b) viscosity measurements (error bars based on triplicate runs); (c) normalized absorbance spectra (recorded using a 0.01 mm path length cuvette) for DTDPP-A-OH, DTDPP-L-OH, DTDPP-F-OH samples at pH 9 and pH 4.

suggestions for dimer stacks at high pH and fibral aggregates at low pH. This is also accompanied with an increase in the concentration of aggregates at low pH.

In comparison to the three systems with aliphatic amino acids, the DTDPP-F-OH assembles into more extensive structures throughout the entire pH range. Firstly, this is indicated by the Bragg peaks in the SAXS data that show a higher degree of ordering between the structures (Fig. 3a, Fig. S12, Supporting Information). Additionally, the SAXS data are best fit to cylindrical models at all pH values, showing the presence of fibrous structures even above the apparent pK_a value (Tables S11–12, Supporting Information). However, there is still a transition between high and low pH, as is indicated by the combination of a power law model to the cylindrical models which suggests the presence of much longer fibral structures. The viscosity data (Fig. 3b and Fig. S13, Supporting Information) shows shear-thinning behaviour across the whole pH range indicating the presence of structures even above the apparent pK_a value, in agreement with the SAXS data. The viscosity increases with decreasing pH, showing an increase in the size and concentration of structures. The absorbance data shows a distinct change in packing with H-type aggregates above the apparent pK_a value and with J-type aggregates below (Fig. 3c, Figs. S14–15 and Table S13, Supporting Information). Therefore, the DTDPP-F-OH results suggest that the additional interactions that are coming from the aromatic R group influence aggregation even further than the aliphatic R groups to create more complex structures.

Overall, for all these systems, there is a clear change in the supramolecular structures that are dispersed through the sol phases with a simple change in pH. The transition point for the structures is found around the apparent pK_a value in each case. This indicates that charge repulsion plays a central role in forming different aggregates. The changes observed include stacking orientation, structure dimension, and material viscosity. However, it is clear that there is no uniform one type of behaviour for these systems, but that there are differences between the data for the different DTDPP-R-OH depending on the amino acid side chain. It is thesefore possible to tune the aggregates formed as well as the molecular packing for these DTDPPs by careful choice of side chain and pH used.

Several literature examples showcase the effect different aggregates have on the photophysical properties and photo-responsive applications [16,23,41]. In absorbance spectroscopy, the increase in aggregation with a decrease in pH leads to more turbid sols and thus a decrease in absorbance intensity is recorded (e.g., Fig. S15a, Supporting Information). As the pH is decreased, the absorbance maxima shift to longer wavelengths which subsequently extends the absorbance to a wider range of the visible region. For example, there is a ≈80 nm extension from the DTDPP-F-OH monomer to the J-aggregate systems. These bathochromic shifts also result in the onset wavelength shifting to longer wavelengths therefore decreasing the optical gap with a pH decrease. For example, for the DTDPP-F-OH sols, the smaller aggregates at a pH of 6 and higher, have an optical gap (E_{opt}) equal to 1.90 eV whereas for the sols at pH 5 and lower (i.e. larger aggregates), E_{opt} decreases to 1.62 eV (Table S14, Supporting Information). In comparison to the E_{opt} of the monomer at 2.15 eV, this shows that aggregation lowers the gap between ground and excited states significantly.

Emission studies show a generalised decrease in intensity as the pH decreases, although with some fluctuations in the linearity of this trend recorded around the apparent pK_a values of the systems (for example as seen for DTDPP-F-OH in Table S14 and Fig. S16, Supporting Information). While J-aggregates typically have more intense fluorescence than H-aggregates [58], in this case the H- to J-switch (from high to low pH) is accompanied with a significant increase in aggregation. This results in aggregate-induced fluorescence quenching and thus super radiance of the J-aggregates in the low pH sols is not recorded. The emission maxima for the entire pH range of DTDPP-F-OH is around 660 nm despite the 60 nm range for the absorbance maxima. H-aggregates are typically characterised by having a greater Stokes shift than J-aggregates, as is observed for the DTDPP-F-OH pH range (Table S14, Supporting Information). Most importantly, these aggregated systems have a larger Stokes shift (ranging from 98 nm to 153 nm for DTDPP-F-OH sols) than the monomeric systems in organic solvent (≈15 nm for DTDPP-F-OH), which is important to avoid back-scattering of light. Similar results for the emission studies are also recorded when using different excitation wavelengths ranging from 350 nm to 575 nm. The DTDPP-A-OH pH range results in similar trends as the DTDPP-F-OH sols, with emission maxima around 660 nm and Stokes shifts between 137 nm and 161 nm. The DTDPP-V-OH and DTDPP-L-OH pH ranges record some deviations in comparison to the other two DTDPP-R-OH systems, and this is owed to the higher concentrations used to prepare the former two systems which can affect emission data measurements. As monomers in organic solvents, the DTDPP-R-OHs showed similar photoluminescence quantum yields (PLQYs) in dilute dimethyl sulfoxide and tetrahydrofuran solution (81–99 %), except DTDPP-V-OH, which was slightly lower at 67 % and 80 %, respectively (Table S18, Supporting Information). As expected, these values were consistent with other reports of DTDPP-based materials [59,60]. At the aggregated concentrations, all DTDPP-R-OH systems showed minimal emission with PLQYs <4 % at both high (>10) and low (<5) pH (Table S18, Supporting Information). The effect of pH on the PLQY for optically dilute samples was also assessed. Similar values were observed for the DTDPP-R-OH systems at high pH (>10), between 47 and 57 %, which again aligned well with other reports of molecularly dissolved, water-based systems [61]. Switching to low pH (<5) resulted in the same distinct changes in absorbance and emission, and could be easily observed by the naked eye (Fig. S20a and Table S18, Supporting Information). DTDPP-A-OH, DTDPP-L-OH, and DTDPP-F-OH showed a significant decrease in PLQY to 2–6 %, while DTDPP-V-OH only decreased slightly to 38 %

(from 51 %). The higher PLQY suggests that the dilution processes for DTDPP-V-OH, even when maintained at low pH, disrupted the aggregated state (Fig. S20b, Supporting Information). In general, the DTDPP-R-OHs show similar trends in the photophysical properties recorded (Tables S15–S18 and Figs. S17–20, Supporting Information). Overall, the most significant effect is the decrease in the optical gap that occurs on going from monomer to aggregated system, and even further on going from high pH (less aggregated) to low pH (more aggregated). This shows that the increased π-π stacking in the aggregated structures results in a smaller energy threshold required to optically excite the sample.

The electroactivity of the monomeric DTDPP (in organic solvent) and the supramolecular aggregates (in water) was determined by cyclic voltammetry (CV) and square wave voltammetry (SWV). All four DTDPP-R-OH monomers show similar electroactivity with quasi-reversible reduction ($E_{1/2} \approx$ - 1.63 V) and oxidation ($E_{1/2} \approx$ 0.47 V) with a peak-to-peak separation of ≈2.1 V (Figs. S21–S22 and Table S19, Supporting Information). Estimations for the monomer HOMO and LUMO energy levels were calculated at −5.20 eV and −3.20 eV respectively, with a HOMO-LUMO gap at 2.00 eV (Table S20, Supporting Information). For the aggregated samples, the electrochemical data consists of broad featureless bands with high capacitance due to the aggregation state. However, data from the main redox peaks can still be extracted to check for trends in the electroactivity and the HOMO-LUMO gap. Taking the DTDPP-F-OH pH 9 sol as an example (Figs. S23–S24 and Table S21, Supporting Information), the quasi-reversible reduction is at $E_{1/2} \approx$ - 0.97 V while the irreversible oxidation is at 0.84 V. This results in a peak-to-peak separation at ≈ 1.85 V (comparable to $E_{opt} = 1.90$ eV) which already shows improvements from the monomeric system. As the pH is decreased, there is a decrease in redox events and in the current indicating that the structures in the lower pH sols are less electroactive than the higher pH counterparts. This suggests that the more extensive structures at low pH are more stable. Plotting the potential values as a function of pH shows that at pH 4 (a second apparent pK_a value for DTDPP-F-OH) the data deviates from linearity which is a common observance at the pK_a of the analytes [62] (Fig. S25, Supporting Information). In this case, the deviation occurs at the systems secondary apparent pK_a value indicating that the electroactivity of the structures changes drastically as the fibral surface charges have been eliminated. In comparison to the monomers, the supramolecular structures allow for a narrower HOMO-LUMO gap (E_g) at ≈ 1.50 eV (Table 1). From the E_g and E_{opt}, the electron binding energy (E_b) can be calculated which results in a drastic change between the high pH systems and the low pH sols. A small E_b and E_g are crucial for optimized performance in optoelectronic devices as less energy is required for exciton formation (Fig. 4). As organized DPP materials are often used for photoresponsive applications [6,7], testing the electroactivity of the materials while the sample was irradiated by an LED was performed. These experiments showed that there is no drastic change between the excited state and ground state redox potentials, with some changes being observed for the peak currents (Figs. S26–S27, Supporting Information). Overall, the low pH samples show the least amount of change, further contributing to the conclusion that these structures are more stable.

The other DTDPP-R-OH materials show similar trends with quasi-reversible reductions and irreversible oxidations that shift to more positive potentials as the pH is decreased (Figs. S28–S42 and Tables S22–S25, Supporting Information) although for DTDPP-V-OH and DTDPP-L-OH, the oxidation potentials shift outside the potential window therefore the HOMO and LUMO energy levels could not be calculated. For DTDPP-A-OH, a decrease in current and electroactivity is observed with a decrease in pH therefore showing that the low pH structures are less prone to redox activity. Additionally, the HOMO-LUMO gap was calculated at 1.60 eV for the pH 9 to pH 6 sols with an E_b at around 0.40 eV. For the irradiated electrochemical measurements, minimal shifts in peak potentials and peak currents were recorded.

Absorbance spectroelectrochemistry (abs-SPEC) measurements were carried out for the DTDPP-R-OH pH ranges to test for radical formation. As both reduction and oxidation potentials are applied, the absorbance spectra exhibit minimal changes from the data recorded with no applied potential (Figs. S43–S50, Supporting Information). No increase or decrease of absorbance peaks are observed as is recorded for similar systems [63]. This is suspected to be due to the highly concentrated samples for abs-SPEC.

In the previous DTDPP-R-OH hydrogel paper, it was observed that the different amino acid R groups provide differences in the packing of the fibral structures into the 3D network at low pH [45]. Herein, the different amino acid R groups manifest into greater variations for the supramolecular structures that are accessible at different pHs. Focusing first on the aliphatic R groups, above the apparent pK_a value these result in dimer or oligomer stacks with a radius of ≈15 Å (Tables S2, S5, and S9, Supporting Information). Below the apparent pK_a value, the fibral structures vary greatly from 140 Å to 34 Å (Tables S3, S6, and S10, Supporting Information). In contrast, the aromatic R group leads to the formation of more complex structures throughout the entire pH range (Tables S11 and S12, Supporting Information). These changes in structural dimension are also accompanied with a shift from H- to J-aggregates with the exception of DTDPP-A-OH sols. Overall, it is the increasing complexity of the supramolecular structures that are created by adapting the amino acid R group, and by tuning the pH that is the root of the variation in the photophysical and electrochemical properties discussed above. This is a remarkable outcome considering that all four DTDPP-R-OHs are based on the same chromophore.

Table 1
Onset potentials, HOMO and LUMO energy levels, and energy gap values for the DTDPP-F-OH pH range.

pH	E_{onset} oxidation (V)	E_{onset} reduction (V)	E_{HOMO} (eV)	E_{LUMO} (eV)	E_g (eV)	E_b (eV)
9	0.66	−0.90	−5.46	−3.89	1.57	0.33
8	0.65	−0.88	−5.45	−3.92	1.53	0.37
7	0.65	−0.85	−5.45	−3.95	1.50	0.40
6	0.65	−0.84	−5.45	−3.96	1.49	0.40
5	0.68	−0.83	−5.48	−3.97	1.51	0.16

3. Conclusions

As a conclusion, this work has investigated the shift of aggregate orientation and the modification of aggregate structure for a library of DPPs in an aqueous medium by using a simple pH change. The molecular packing is a consequence of a combination of directional forces between hydrophobic molecules within an aqueous environment (likely driven by H-bonding and, to a lesser extent, π-π interactions), and charge repulsion dictates the orientation of packing and the extent of assembly. Aggregates above the apparent pK_a value adapt orientations that minimise charge repulsion (dimer/oligomer stacks, short fibres) while aggregates below the apparent pK_a value have more extensive packing (laterally aggregated long fibres) due to the elimination of charges.

Most significantly, variations in the photophysical and electrochemical properties are obtained by maintaining the same monomer template and by only changing the pH of the system to alter the aggregation state. Furthermore, changing the linked amino acid group results in property differences despite all DTDPP-R-OH systems being based on the same chromophore unit. Overall, changes in aggregation result in differences in the absorbance range, optical gap, Stokes shift, electroactivity, and HOMO-LUMO gap. The DTDPP-F-OH low pH sol materials have the most extensive packing and thus have the best charge carrier separation and charge transfer properties.

Overall, this work shows how it is possible to synthesize one molecule and then use self-assembly to fabricate various different aggregate types by optimising the pH and avoiding time-consuming, extensive synthetic procedures. Additionally, by taking advantage of self-assembly via the hydrophobic effect and charge repulsion, the fabrication of

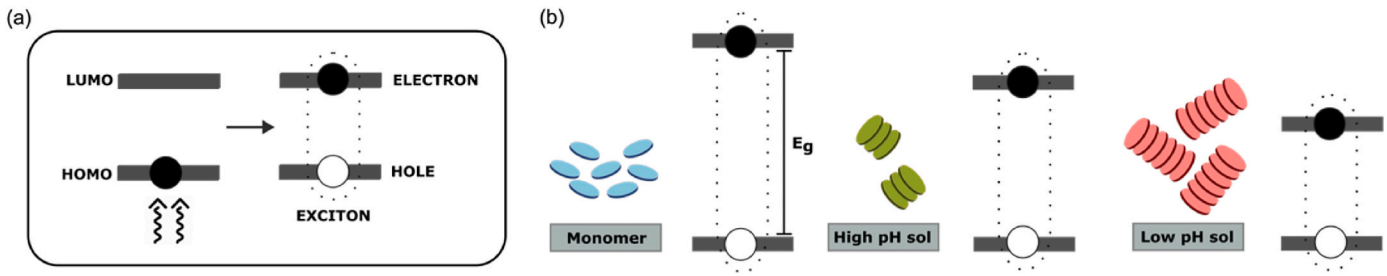

Fig. 4. Cartoon representation of (a) photoresponsive exciton formation and (b) E_g optimisation from different assembled states that favour exciton formation.

different structures can be achieved in an environmentally-benign aqueous matrix. This work is important for photoresponsive applications as more complex aggregates require less energy for exciton formation due to the intermolecular orbital overlap achieved from increased π-π stacking.

4. Experimental

The DTDPP-R-OH were prepared as described elsewhere [45]. The DTDPP-R-OH powders (synthesized from reagents purchased from Merck, Fluorochem or TCI) were dissolved in deionised water with two equivalents of 1 M NaOH (Sigma Aldrich). These samples were stirred overnight until a clear, dark red solution was achieved at a pH value of 10.5. The DTDPP-R-OH sols were prepared at different pH values starting from the pH 10.5 starting solution by the addition of acid (0.1 M, 1 M, or 2 M HCl; Sigma Aldrich) while vigorously stirring the sample at 1500 rpm (Note: vigorous stirring is essential to prevent the formation of large hydrogel clusters and to form a visibly homogenous sol). The materials prepared at the mgc were at concentrations of 5 mg/mL for DTDPP-F-OH and DTDPP-A-OH, 10 mg/mL for DTDPP-V-OH, and 15 mg/mL for DTDPP-L-OH.

A FC200 pH probe (HANNA instruments) was used to measure the pH values of the DTDPP-R-OH sols. The probe was calibrated prior to use with pH 10, pH 7, and pH 4 buffer solutions (HANNA instruments).

SAXS experiments were carried out at the B21 beamline at Diamond Light Source, UK. This beamline operates at a fixed energy of 12.4 keV and a camera length of 4.014 m, resulting in a Q range of 0.004–0.44 $Å^{-1}$.

Viscosity data was recorded using an Anton Paar Physica MCR101 rheometer. Measurements were performed using a 50 mm cone geometry (CP50 – cone angle = 0.994°) with gap distance between the geometry and the flat rheometer plate set to 0.1 mm. Samples (pH 10.5 solutions) were poured onto the aluminium flat plate for measurement directly from the falcon tube. The temperature was set to 25°C. Measurements were performed in triplicate, with a fresh sample for each run. The values for the data points were averaged, and the standard deviation is calculated and shown as error bars on the graphs.

UV–Vis absorbance spectra were recorded using a Agilent Cary 60 spectrophotometer. Data was recorded by performing a baseline correction with the deionised water before recording the spectra for the sample. Spectra were recorded with a 10 or 0.01 mm path length quartz cell (Hellma Analytics). Fluorescence emission spectra were recorded using an Agilent Cary Eclipse fluorescence spectrophotometer. Measurements investigating the effect of pH change were obtained using a 10 mm path length quartz cell (Hellma Analytics) and were recorded with a 20 nm excitation slit and a 20 nm emission slit. Measurements for the optically dilute samples (absorbance ≈0.1 at λ_{exc}) were recorded on an Agilent Cary Eclipse fluorescence spectrophotometer using a 10 mm path length quartz cell (Hellma Analytics) and were recorded with a 5 mm excitation slit and a 10 mm emission slit. Measurements of the photoluminescence quantum yield were recorded on a Edinburgh Instruments FS5 instrument using a SC-30 integrating sphere.

Cyclic voltammetry and Square Wave Voltammetry measurements were performed using a CH Instruments Electrochemical Workstation (CHI 440a), Austin, TX, USA. Monomer samples were prepared in dry DMF (Sigma Aldrich) at a concentration of 0.3 mg/mL with 0.1 M tetrabutylammonium hexafluorophosphate (TBAP, electrochemistry grade, Sigma Aldrich). Sol samples were prepared as described above and with 0.1 M NaCl (Sigma Aldrich) as supporting electrolyte. The experiments made use of a three-electrode setup; a glassy carbon working electrode, a Pt wire counter electrode and a 3 M NaCl Ag/AgCl reference electrode (for aqueous experiments) or a Pt wire pseudoreference electrode (with added ferrocene, for organic solvent experiments). All samples were purged with N_2. Measurements for the irradiated CV and SWV experiments were made with a white LED (Oslon, 340 lumens, 700 mA, 5000K temperature) attached to a heat sink. The LED bulb was positioned 2 cm from the bottom of the glass vessel (Fig. S49).

Spectroelctrochemistry measurements were performed using a combination of a Shimadzu UV-3600 spectrophotometer and a CH Instruments Electrochemical Workstation (CHI 440a). A BASi spectroelectrochemical kit was used (a quartz cuvette, a Pt mesh working electrode, a Pt wire counter electrode and an Ag/AgCl (3 M KCl) reference electrode). Absorption spectra were reorded one minutre after the desired potential was applied.

CRediT authorship contribution statement

Valentina Gauci: Writing – review & editing, Writing – original draft, Methodology, Investigation, Formal analysis, Data curation, Conceptualization. **Alex S. Loch:** Data curation, Formal analysis. **Daniel McDowall:** Writing – review & editing, Methodology, Investigation. **Charlotte Edwards-Gayle:** Writing – review & editing, Methodology, Investigation. **Dave J. Adams:** Writing – review & editing, Writing – original draft, Supervision, Resources, Project administration, Methodology, Funding acquisition, Formal analysis, Conceptualization.

Declaration of competing interest

The authors declare the following financial interests/personal relationships which may be considered as potential competing interests: Dave J. Adams reports financial support was provided by Engineering and Physical Sciences Research Council. Dave J. Adams reports financial support was provided by Leverhulme Trust. If there are other authors, they declare that they have no known competing financial interests or personal relationships that could have appeared to influence the work reported in this paper.

Data availability

Data will be made available on request.

Acknowledgements

We thank Michele Cariello for assistance with the set up for the electrochemical measurements. We thank the Leverhulme Trust for

funding (RPG-2019-165 and RPG-2018-013). We thank the EPSRC (R03480X/1) for funding. We acknowledge STFC beamtime allocation SM29985 on B21 at Diamond. This work benefitted from the SasView software, originally developed by the DANSE project under NSF award DMR-0520547.

Appendix A. Supplementary data

Supplementary data to this article can be found online at https://doi.org/10.1016/j.dyepig.2024.111968.

References

[1] Behnke M, Tieke B. Langmuir 2002;18:3815–21.
[2] Gao Y, Feng G, Jiang T, Goh C, Ng L, Liu B, Li B, Yang L, Hua J, Tian H. Adv Funct Mater 2015;25:2857–66.
[3] Beyerlein T, Tieke B. Macromol Rapid Commun 2000;21:182–9.
[4] Wang L, Lai B, Ran X, Tang H, Cao D. Molecules 2023;28:4097.
[5] Li W, Wang L, Tang H, Cao D. Dyes Pigments 2019;162:934–50.
[6] Qu S, Tian H. Chem Commun 2012;48:3039–51.
[7] Ghosh S, Shankar S, Philips DS, Ajayaghosh A. Mater Today Chem 2020;16:100242.
[8] Szabadai RS, Roth-Barton J, Ghiggino KP, White JM, Wilson DJD. Aust J Chem 2014;67:1330–7.
[9] Dhar J, Venkatramaiah N, A A, Patil S. J Mater Chem C 2014;2:3457–66.
[10] Suna Y, Nishida J-i, Fujisaki Y, Yamashita Y. Org Lett 2012;14:3356–9.
[11] Yue J, Liang J, Sun S, Zhong W, Lan L, Ying L, Yang W, Cao Y. Dyes Pigments 2015;123:64–71.
[12] Podlesný J, Dokládalová L, Pytela O, Urbanec A, Klikar M, Almonasy N, Mikysek T, Jedryka J, Kityk IV, Bureš F. Beilstein J Org Chem 2017;13:2374–84.
[13] Dou L, Liu Y, Hong Z, Li G, Yang Y. Chem Rev 2015;115:12633–65.
[14] Bürckstümmer H, Weissenstein A, Bialas D, Würthner F. J Org Chem 2011;76:2426–32.
[15] Cheng P, Yang Y. Acc Chem Res 2020;53:1218–28.
[16] Militzer S, Thi My Phuong T, Mesini PJ, Ruiz-Carretero A. ChemNanoMat 2018;4:790–5.
[17] Ponnappa SP, Arumugam S, Spratt HJ, Manzhos S, O'Mullane AP, Ayoko GA, Sonar P. J Mater Res 2017;32:810–21.
[18] Grzybowski M, Gryko DT. Adv Opt Mater 2015;3:280–320.
[19] Grzybowski M, Hugues V, Blanchard-Desce M, Gryko DT. Chem Eur J 2014;20:12493–501.
[20] Mizuguchi J, Imoda T, Takahashi H, Yamakami H. Dyes Pigments 2006;68:47–52.
[21] Thool GS, Narayanaswamy K, Venkateswararao A, Naqvi S, Gupta V, Chand S, Vivekananthan V, Koner RR, Krishnan V, Singh SP. Langmuir 2016;32:4346–51.
[22] Li Y, Sonar P, Murphy L, Hong W. Energy Environ Sci 2013;6:1684–710.
[23] Lee OP, Yiu AT, Beaujuge PM, Woo CH, Holcombe TW, Millstone JE, Douglas JD, Chen MS, Frechet JMJ. Adv Mater 2011;23:5359–63.
[24] Spano FC. Acc Chem Res 2010;43:429–39.
[25] Kao KC. In: Kao KC, editor. Dielectric phenomena in solids. San Diego: Academic Press; 2004. p. 381–514.
[26] Zou X, Cui S, Li J, Wei X, Zheng M. Front Chem 2021;9:671294.
[27] Fu C, Beldon PJ, Perepichka DF. Chem Mater 2017;29:2979–87.
[28] Kitisriworaphan W, Chawanpunyawat T, Manyum T, Chasing P, Namuangruk S, Sudyoadsuk T, Promarak V. RSC Adv 2021;11:12710–9.
[29] Głowacki ED, Coskun H, Blood-Forsythe MA, Monkowius U, Leonat L, Grzybowski M, Gryko D, White MS, Aspuru-Guzik A, Sariciftci NS. Org Electron 2014;15:3521–8.
[30] Ávila-Rovelo NR, Martinez G, Matsuda W, Sinn S, Lévêque P, Schwaller D, Mésini P, Seki S, Ruiz-Carretero A. J Phys Chem C 2022;126:10932–9.
[31] Wang A, Shi W, Huang J, Yan Y. Soft Matter 2016;12:337–57.
[32] Tantakitti F, Boekhoven J, Wang X, Kazantsev RV, Yu T, Li J, Zhuang E, Zandi R, Ortony JH, Newcomb CJ, Palmer LC, Shekhawat GS, de la Cruz MO, Schatz GC, Stupp SI. Nat Mater 2016;15:469–76.
[33] Raeburn J, Cardoso AZ, Adams DJ. Chem Soc Rev 2013;42:5143–56.
[34] Kirkus M, Wang L, Mothy S, Beljonne D, Cornil J, Janssen RAJ, Meskers SCJ. J Phys Chem A 2012;116:7927–36.
[35] Tamayo AB, Tantiwiwat M, Walker B, Nguyen T-Q. J Phys Chem C 2008;112:15543–52.
[36] Adachi M, Nakamura S. J Phys Chem 1994;98:1796–801.
[37] Iqbal A, Jost M, Kirchmayr R, Pfenninger J, Rochat A, Wallquist O. Bull Soc Chim Belg 1988;97:615–44.
[38] Mizuguchi J. J Phys Chem A 2000;104:1817–21.
[39] Aytun T, Barreda L, Ruiz-Carretero A, Lehrman JA, Stupp SI. Chem Mater 2015;27:1201–9.
[40] Shin W, Yasuda T, Watanabe G, Yang YS, Adachi C. Chem Mater 2013;25:2549–56.
[41] Mas-Montoya M, Janssen RAJ. Adv Funct Mater 2017;27.
[42] Pop F, Lewis W, Amabilino DB. CrystEngComm 2016;18:8933–43.
[43] Biswas S, Kumar M, Levine AM, Jimenez I, Ulijn RV, Braunschweig AB. Chem Sci 2020;11:4239–45.
[44] Gevaerts VS, Herzig EM, Kirkus M, Hendriks KH, Wienk MM, Perlich J, Müller-Buschbaum P, Janssen RAJ. Chem Mater 2014;26:916–26.
[45] Gauci V, Seddon A, Adams DJ. Soft Matter 2022;18:3756–61.
[46] Draper ER, Dietrich B, Adams DJ. Chem Commun 2017;53:1864–7.
[47] Frisch H, Besenius P. Macromol Rapid Commun 2015;36:346–63.
[48] Tang C, Smith AM, Collins RF, Ulijn RV, Saiani A. Langmuir 2009;25:9447–53.
[49] Tang C, Ulijn RV, Saiani A. Langmuir 2011;27:14438–49.
[50] Chen L, Revel S, Morris K, Serpell LC, Adams DJ. Langmuir 2010;26:13466–71.
[51] McDowall D, Greeves BJ, Clowes R, McAulay K, Fuentes-Caparros AM, Thomson L, Khunti N, Cowieson N, Nolan MC, Wallace M, Cooper AI, Draper ER, Cowan AJ, Adams DJ. Adv Energy Mater 2020;10.
[52] Draper ER, Dietrich B, McAulay K, Brasnett C, Abdizadeh H, Patmanidis I, Marrink SJ, Su H, Cui H, Schweins R, Seddon A, Adams DJ. Matter 2020;2:764–78.
[53] Kasha M. Radiat Res 1963;20:55–70.
[54] Hochstrasser RM, Kasha M. Photochem Photobiol 1964;3.
[55] Kasha M, Rawls HR, El-Bayoumi MA. Pure Appl Chem 1965;11:371–92.
[56] Spano FC, Silva C. In: Johnson MA, Martinez TJ, editors. Ann. Rev. Phys. Chem., 65; 2014. p. 477–500.
[57] Hestand NJ, Spano FC. Chem Rev 2018;118:7069–163.
[58] Spano FC, Mukamel S. J Chem Phys 1989;91:683–700.
[59] Choi M-W, Kim G, Seitkazina A, Kim S-Y, Yoon WS, Kwon JE, Kim S, Park SY. Dyes Pigments 2022;207:110699.
[60] Cigánek M, Heinrichová P, Kovalenko A, Kučerík J, Vala M, Weiter M, Krajčovič J. Dyes Pigments 2020;175:108141.
[61] Heyer E, Lory P, Leprince J, Moreau M, Romieu A, Guardigli M, Roda A, Ziessel R. Angew Chem Int Ed 2015;54:2995–9.
[62] Brownson DAC, Banks CE. In: Brownson DAC, Banks CE, editors. The handbook of graphene electrochemistry. London: Springer London; 2014. p. 23–77. https://doi.org/10.1007/978-1-4471-6428-9_2.
[63] Gora M, Pluczyk S, Zassowski P, Krzywiec W, Zagorska M, Mieczkowski J, Lapkowski M, Pron A. Synth Met 2016;216:75–82.